Effect of Power Distribution Change on T/H Parameters by using CUPID

Eun Hyun Ryu [a*] and Jong Yub Jung [a]
[a]*Korea Atomic Energy Research Institute, 1045 Daedeok-daero, Yuseong-gu, Daejon, 34057, Korea*
[*]*Corresponding author: ryueh@kaeri.re.kr*

1. Introduction

Several studies have addressed pressure tube deformation on neutronics behavior. Through those studies, we determined pressure tube deformation changes pin power distribution including fission product build up change, coolant void reactivity(CVR) change and so on. However, all these results are only about neutronics behavior. Thus, if we want to know about the impact of pressure tube deformation on safety parameters, we should use T/H calculations reflecting those changes. Among changes which come from pressure tube deformation, the pin power distribution is the most powerful factor on the safety parameters. Because it is difficult to incorporate the neutronics feedback effect, we used the CUPID only calculation in this study to reveal the sensitivity of the power distribution.

The CUPID code was developed in a division of the Korea Atomic Energy Research Institute(KAERI) and has been continuously maintained. The CUPID code as a multiscale code, can be used for both subchannel and CFD scale calculations.

Because the most important issue in channel safety is the critical heat flux (CHF), we calculated and analyzed three parameters that have a critical effect on the CHF. In addition to the three major parameters, the mass flow rate, pressure and quality, we also analyzed other parameters, namely, the solid and fluid temperatures and fluid densities.

2. Problem Description

2.1 Geometry

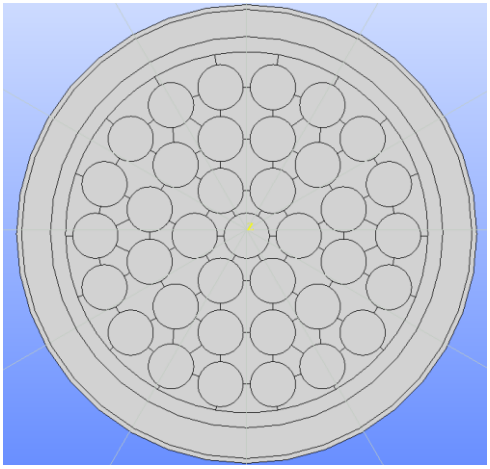

Fig. 1. Cross Sectional View of the Problem

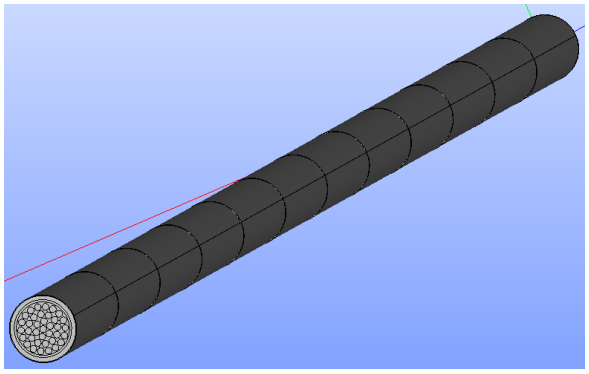

Fig. 2. Overall View of the Problem

As shown in Fig. 1 and Fig. 2, various appendages which exist in the real channel were omitted in this analysis. In addition, although a power change actually occurs with deformed geometry, we assumed that only the power distribution changes.

Due to the weight of the fuel itself and gravity, the fuel location was positioned downward a little as soon as it was loaded to the core as is evident in Figs. 1 and 2.

CATIA modeling was done, first. Then the STP file format was exported after modeling. The Salome program was then used to import the prototype modeling and to mesh the model.

2.2 Material

Table I: Material Assignment of CUPID Calculation

	Reality	CUPID
Fuel	UO_2+He+Zr-4	Volume Weighted Material (solid 10)
Coolant	D_2O(99% purity)	D_2O
Pressure Tube	Zr-Nb	Stainless Steel (solid 4)
Gap	CO_2	Air (ncg 6)
Calandria Tube	Zr-2	Stainless Steel (solid 4)

As shown in Fig. 1 and Fig. 2, the fuel, gap and cladding were unified as one region. Volume weighted integration was carried out during the merging process, and instead of Zircaloy, stainless steel was used for the pressure tube and the calandria tube. In a real core, CO_2 is used for the gap between the pressure tube and the calandria tube. However, in this study, it was difficult to implement CO_2, so instead of CO_2, we used air.

2.3 Mesh

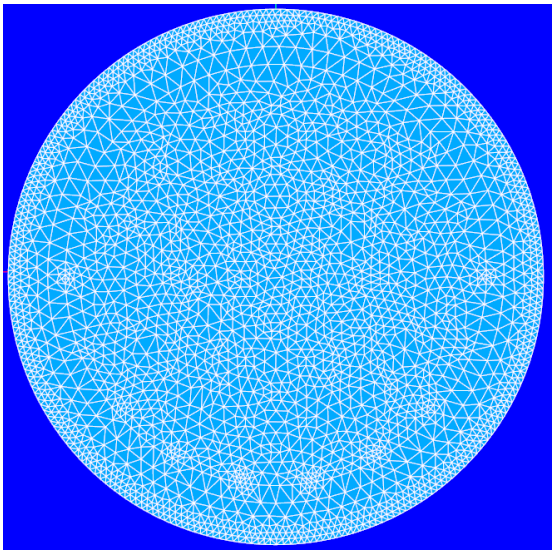

Fig. 3. Cross Sectional View of the Mesh

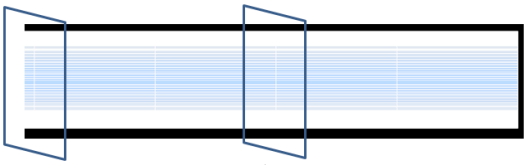

Fig. 4. One End of the Channel(2 Axial Nodes for 1 Bundle)

A total of 36,600 nodes, 119,472 (prism, 4978 X 24) volumes, and 24 axial levels in 3-D space were used as well as 4,978 triangles in the radial direction as shown in Fig. 3 and Fig. 4. To have this mesh, 2-dimensional extrusion was used with Salome software.

2.4 Boundary Condition

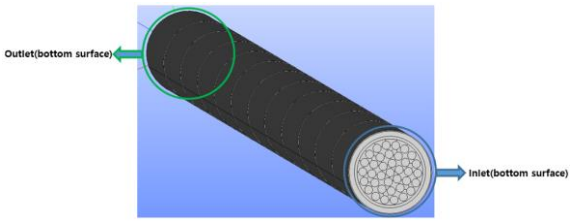

Fig. 5. Top and Bottom Surfaces(Outlet and Inlet)

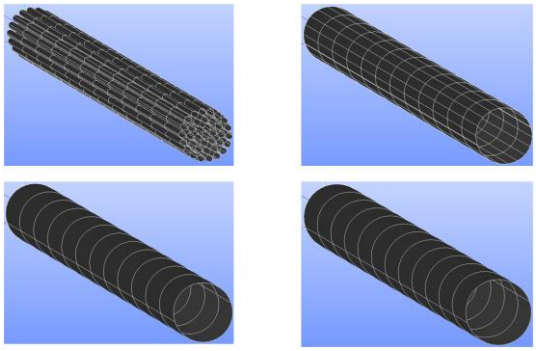

Fig. 6. Surfaces for Solid and Fluid Interface

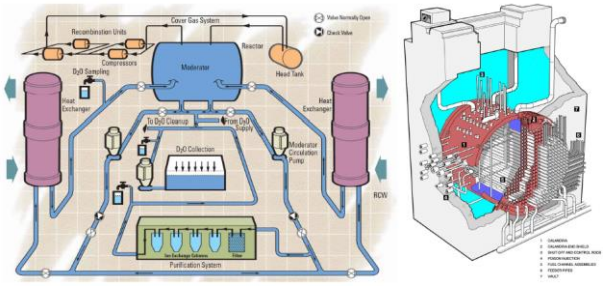

Fig. 7. Schematic View of Moderator System

Although in reality, there is heat loss through solid surfaces in the top and bottom surfaces, we assumed that there was no conduction heat loss through these surfaces. As shown in Fig. 5, we had 2 fluid regions, main heavy water coolant and the non-condensible gas through the gap between the pressure tube and the calandria tube

Radial heat transfer is possible for the surfaces that are shown in Fig. 6. The ultimate heat sink of the channel is the moderator in the end, because the moderator's temperature is maintained at 69 degrees celsius with an independent moderator system as shown in Fig. 7 [1,2].

2.5 Power Profile

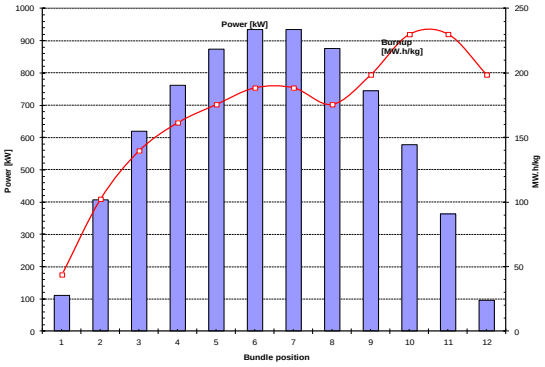

Fig. 8. Axial Power and Burnup Profiles

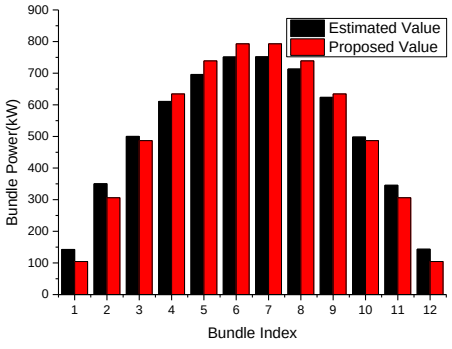

Fig. 9. Estimated and Proposed Axial Powers

Although axial power distribution is not symmetric as shown in Fig. 8 and Fig. 9, rather the inlet is skewed, and the tested axial power profile is nearly symmetric. This is because the degree of skew is not that much. As shown in Fig. 9, the difference between the real axial power distribution and proposed, cosine distribution are almost the same. We assumed that this axial power distribution did not change.

Table II: Bundle Power Distribution at Average Bundle Discharge Burnup(1600Wh/kg(U))

Element Ring	Number of Elem.	Element Power		Percent Power	
		Nor. To Bun. Avg.	Nor. To Outer Elem.	Per Elem.	Per Ring
Outer	18	1.120	1.000	3.026	54.46
Inter.	12	0.9254	0.8266	2.501	30.01
Inner	6	0.8247	0.7367	2.229	13.37
Center	1	0.7843	0.7006	2.120	2.120

Table II shows, the radial distribution. For the second case, the radial power distribution in the 5th column (per elem.) was changed to 2.99, 2.45, 2.4, 2.38 artificially.

It is known that the increased coolant volume reduces the pin power around the coolant. Thus the outer pins have lower power. For the same reason, pins in low elevation have larger power.

The RMS difference between the pin power for reference-case that power is not changed. and the deformed case was set as about 3.6%.

2.6 T/H Condition

Because we have two fluid zones in the problem modeling, there are two T/H conditions for each fluid zone. All values can be found in several documents such as the physics design manual [3], except for the gap region. No pressure drop could be found, so the current temporal value was set. However, it was close to the atmospheric pressure, so maybe there was no impact from the outlet pressure of the gap region on the results. As shown in Table III and Table IV, there was no heavy water in the second region because we had a void fraction of 1.0 and NCG quality of 1.0.

Table III: T/H Values for Coolant Region

	Initial Value	Inlet Condition	Outlet Condition
Pressure (Pa)	11.4E6		10.0E6
Liq. Temp. (Kelvin)	535.61		N/A
Gas Temp. (Kelvin)	535.61		N/A
Void Fraction	0.0		N/A
NCG Quality	0.0		0.0
Velocity (m/s)	8.3229		N/A

Table IV: T/H Values for Gap (CO_2) Region

	Initial Value	Inlet Condition	Outlet Condition
Pressure (Pa)	221325		201325
Liq. Temp. (Kelvin)	451.65		N/A
Gas Temp. (Kelvin)	451.65		N/A
Void Fraction	1.0		N/A
NCG Quality	1.0		0.0
Velocity (m/s)	16.6458		N/A

2.7 Iteration Conditions

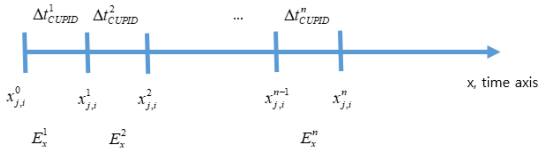

Fig. 10. Time Axis and Error Conditions

$$E_x^n = \frac{1}{\Delta t_{CUPID}^n}\sqrt{\frac{\sum_{i=1}^{12}\sum_{j=1}^{p(x)} V_{j,i}(x)\left(x_{j,i}^n - x_{j,i}^{n-1}\right)}{\sum_{i=1}^{12}\sum_{j=1}^{p(x)} V_{j,i}(x)}}, \left\{x = T_{solid}, T_{fluid}, \rho_{fluid}\right\} \quad (1)$$

$$C_x > E_x^n \quad (2)$$

where, n is the time index, i is the bundle index, j is the radial region index, delta t is the size of the time inverval which is used in the CUPID code, E is the self-determined error parameter, C is the self-determined convergence criteria which is currently set as 0.3, 0.2, 0.4.

The convergence speed of the solid temperature was the slowest compared with the fluid temperature and the density. The setting the convergence criteria of the solid temperature was the most important. In this study, we intended that the error parameter incorporate the concept of the change rate per second. Thus, we regarded that 0.3 degree per second was a sufficient magnitude to accept the result.

3. Numerical Results

The Windows version of the CUPID code was used in this study. The CPU specifications of the calculation resource were intel core™ i7-8700 CPU @3.20GHz

3.19GHz. We had 2 threads per core, and hyper threading was set as auto. Because implicit calculation was not possible, the calculation time was as long as 6 days for each case.

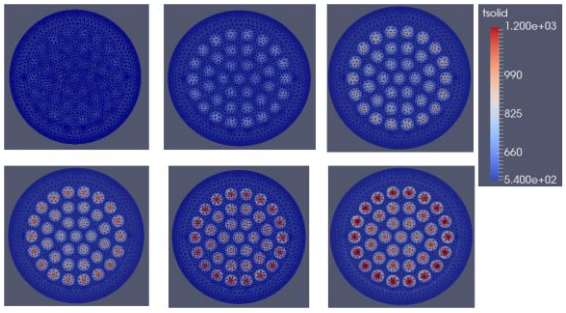

Fig. 11. Fuel Temperature of Plane 1~6

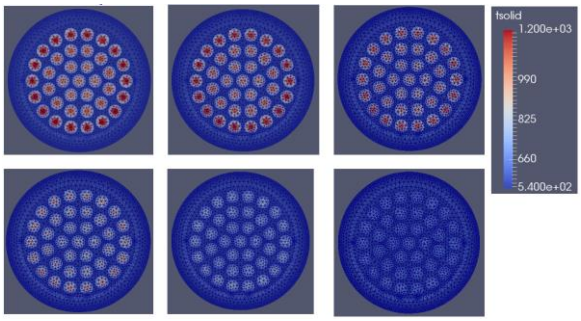

Fig. 12. Fuel Temperature of Plane 7~12

Fuel temperatures were not exactly symmetric along the axial axis because the fluid temperature near the inlet was much lower than that of the fluid temperature near the outlet. Thus, the heat transfer between the solid and fluid near the inlet was much greater than that near the outlet. As shown in Fig. 11 and Fig. 12, the fuel temperature looks had a cosine shape because the axial power was set as cosine shape. In addition, from inside to outside, we can observe that the pin power increased for that direction.

Table V: Comparison of Pressure Tube Temperatures

Bundle Index	PT (38-th solid Region)		
	PDM (K)	CUPID	
		Reference Case (K)	Deformed Case (K)
1	561.2	534.0	534.0
2		535.7	535.7
3		538.9	538.9
4		543.4	543.3
5		548.6	548.5
6		554.3	554.1
7		559.8	559.6
8		565.0	564.8
9		569.7	569.3
10		573.3	572.9
11		575.6	575.2
12		576.5	576.0
Average	561.2	556.2	556.0

Table VI: Comparison of Calandria Tube Temperatures

Bundle Index	PT (38-th solid Region)		
	PDM (K)	CUPID	
		Reference Case (K)	Deformed Case (K)
1	342.15	342.7	342.7
2		342.6	342.6
3		342.6	342.6
4		342.6	342.6
5		342.6	342.6
6		342.6	342.6
7		342.6	342.6
8		342.6	342.6
9		342.7	342.7
10		342.7	342.7
11		342.7	342.7
12		342.7	342.7
Average	342.15	342.6	342.6

We had 39 solid regions for the axial level: 37 fuel pins, a pressure tube and a calandria tube. Among the 39 solid regions, as shown in Table V and Table VI, the calculated temperatures of the pressure tube and the calandria tube well matched the reference values, which were taken from the physics design manual [3].

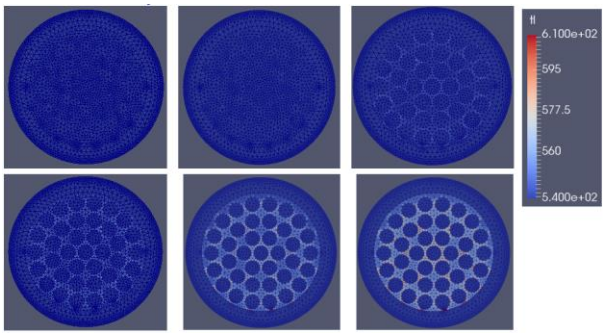

Fig. 13. Fluid Temperature of Plane 1~6

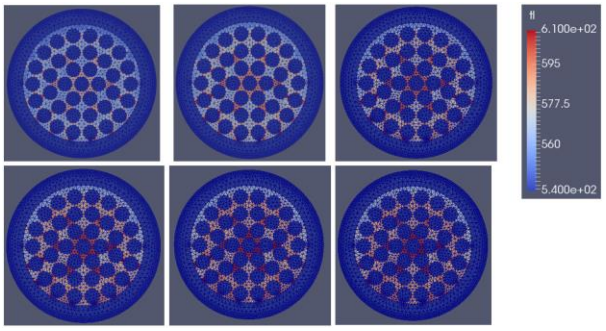

Fig. 14. Fluid Temperature of Plane 7~12

There are 61 fluid regions for an axial level. Among the 61 fluid regions, 60 fluid regions are for heavy water coolant and the 61-th region is for the CO_2 gas gap region between the pressure tube and the calandria tube.

Of course, the fluid temperature rises along the axial direction because the heat transferred from the solid is accumulated as time goes on (as axial elevation increases). It is also natural that regions with small flow areas compared with the neighbor fuel pin position will have a much higher temperature compared with that of the other regions. Specific to the channel design, the central subchannel regions around the center fuel pin have smaller flow areas, and subchannel regions in the bottom part have smaller flow areas as well. This is due to the design specifications and fuel sagging owing to the weight of the fuel itself.

Table VII: Global Errors for Fuel and Fluid Temperatures and Fluid Density

	Fuel Temp.	Fluid Temp.	Fluid Density
RMSE	8.49K	0.99K	2.66kg/m^3
MAXE	4.17% (34.04K)	0.79% (4.63K)	0.33% (2.53kg/m^3)
MAXE Pos.	7-th Bundle, 1-th Fuel	8-th Bundle, 6-th S.C.	8-th Bundle, 22-th S.C.
MINE	-1.03% (-8.66K)	-0.16% (-0.92K)	-1.82% (-13.72kg/m^3)
MINE Pos.	6-th Bundle, 8-th Fuel	8-th Bundle, 22-th S.C.	8-th Bundle, 6-th S.C.

In Table VII, RMSE, MAXE, Pos., MINE, Temp, S.C. are the root mean square error, maximum error, position, minimum error, temperature, and subchannel, respectively.

By considering that the power change is enlarged compared with the magnitude of the real aged channel power, the global changes shown in Table VII should be approximately divided by 6. Them we can see that the fuel temperature, coolant temperature, and coolant density changes are globally just about 1.4K, 0.16K, and 0.44kg/m_3 as well as MAXE and MINE.

4. Conclusion

Even though the actual approximated power distribution change was evaluated as 0.5% of the RMSE, we set over 3% of the RMSE to amplify the result. As a result, we obtained the global change as shown in Table VII and the detailed cell-wise results as shown in Figures 11~14 and Tables V and VI. However, various results reveals that the magnitude of 3 major results, namely, as fuel temperature, fluid temperature and fluid density, are extremely small. In addition, we should divide by about 6 by considering that we amplify the input. By taking this fact into account, the pin power change itself has almost no impact on the safety parameters. Because that feedback and the geometrical effects are not considered here, note that mere power change is dealt with in this study.

Acknowledgement

This work was supported by the National Research Foundation of Korea (NRF) grant funded by the Korea Government (Ministry of Science and ICT) (No. NRF-2017M2A8A4017282)

REFERENCES

[1] H. K. Cho, Nuclear Systems Enginnering Lecture Material 1-1, 2017.
[2] H. K. Cho, Nuclear Systems Engineering Lecture Material 1-2, 2017.
[3] KHNP, CANDU 6 Generating Station Physics Design Manual, 2009.